

MASSACHUSETTS INSTITUTE OF TECHNOLOGY

DEPARTMENT OF PHYSICS

CAMBRIDGE, MASSACHUSETTS 02139

1 December 1978

Dear John,

Enclosed is a final report for the Phase-A Cobe Study. It includes studies of the following:

Diffraction patterns of the apodizing Horn,

Calculations of the trade off between noise and spectral resolution for the FIRAS,

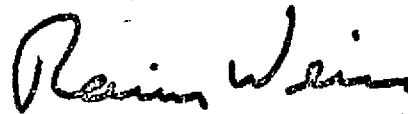
A preliminary study on flexural transports,

An optical study of the Martin-Pupplet polarizing interferometer,

A study of radiation absorption of thin Bismuth films.

The interim Phase-A study report is also part of the output of this contract.

Sincerely yours,



Rainer Weiss  
Professor of Physics



(NASA-TM-84037) PHASE-A COBE STUDY Final  
Report (Massachusetts Inst. of Tech.) 57 p  
HC A04/MF A01 CSCI 20N

N82-10288

Unclas  
G3/32 39302

## MULTI-MODE HORN TESTS

A scaled version of a conical apodizing horn similar to the design to be used in COBE as the antenna for the FIRAS was constructed at MIT and tested at JPL.

The cylindrical horn was constructed of brass tubing and sheet stock. The cone shown in Figure 1 is comprised of a straight conical section 110 cm long with a total cone angle of  $7^\circ$  beginning at the small end with a diameter of 0.711 cm and ending in a diameter of 14.1 cm. The large diameter is mated to a toroidal spinning with cylindrical radius of 15.2 cm flaring from 14.1 cm to 44.1 cm at the output. The toroid is cut so that the tangent at the open end of the flare is  $90^\circ$  to the cone axis. The toroidal piece was provided by David Woody at Berkeley.

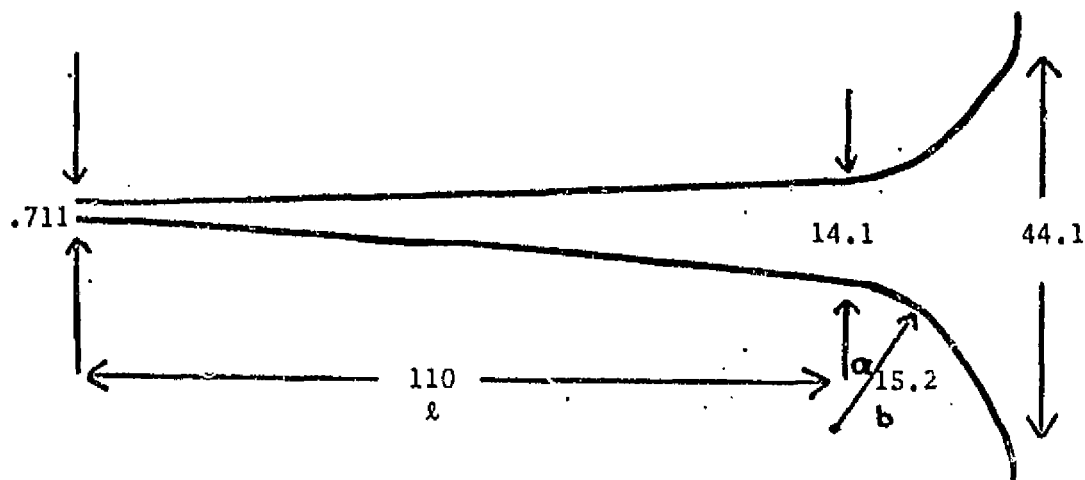


Figure 1

The small end of the cone was attached to a rectangular wave guide RG 96/U. The transition from the cylindrical  $TE_{11}$  to the rectangular  $TE_{01}$  modes was abrupt which results in a mismatch roughly proportional to the

ratio of the overlapping areas of the two waveguides to the area of the rectangular guide - 2 db.

The horn tests and results are described in the attached report by S. Bednarczyk of JPL.

The angular width of the central maximum of the antenna pattern as given by geometric optics is the total cone angle for a horn of this length. The observed width at the 1/2 power points is 6° FWHM independent of the polarization of the incoming wave which is in substantial agreement with the 7° FWHM prediction. The antenna pattern follows the Airy function of an open hole of diameter 14 cm which is the diameter at the transition between the straight cone and the toroidal section. The crawling waves of the Keller Theory dominate at angles larger than 15°.

The Airy function describes the diffraction by a circular hole:

$$\frac{I(\theta)}{I(0)} = \left[ \frac{2J_1(x)}{x} \right]^2$$

where  $x = \frac{2\pi a}{\lambda} \sin \theta$ .

For  $x > 10$ :

$$\frac{I(\theta)}{I(0)} = \frac{8}{\pi x^3} \cos^2 \left( x - \frac{3\pi}{4} \right)$$

For the test horn:

$$\lambda = .97 \text{ cm} \quad a = 7.05 \text{ cm} \quad x = 45.6 \sin \theta$$

The zeroes in the Airy function occur at:

<u>x</u>	<u><math>\theta</math>(deg)</u>
3.83	4.81
7.016	8.84
10.173	12.88
13.324	16.97
16.49	21.17
19.63	25.46
22.77	29.91
25.92	34.59
29.06	39.52
32.20	44.84
35.34	50.74
38.48	57.4
41.63	65.7
44.77	78.6

The extended Airy pattern is best seen in the  $E_{\perp}$  plots.

The Keller Theory applied to the horn is taken from Keller (J. Appl. Phys., Vol. 30, p. 1452, 1959); and the attachment coefficients, from the MIT senior thesis of J. Anderson and A. Szymkowiak (MIT Physics Dept., 1976).

The ratio of the intensity diffracted into an angle  $\theta$  to the intensity of the undiffracted wave going into  $\theta = 0$  is given by:

$$\frac{I(\theta)}{I} = \left( \frac{.22}{.64} \right) \frac{2\theta_{\text{BEAM}} \lambda}{\pi^2 \omega} \left( \frac{b}{\lambda} \right)^{2/3} e^{-\left( \frac{5.93}{2.58} \right) \left( \frac{b}{\lambda} \right)^{1/3} \theta} \quad (11)$$

where  $w$  is the diameter at the transition between straight cone and toroidal section,  $b$  is the cylindrical radius of the torus. The coefficients in the parentheses are taken from Keller and have been experimentally verified to 25% by Anderson and Szymkowiak. The upper coefficient is for  $E_{11}$  and the lower for  $E_1$ .

Both the Airy function and the Keller calculation have been drawn on the data in antenna patterns 4 and 14. For the important case,  $E_{11}$ , the theory overestimates the diffraction at large angles by 3 to 5db.

#### Off-Axis Rejection Required

The main beam covers a solid angle  $\Omega_s$ , the side lobes of the antenna looking into a hot source cover a solid angle  $\Omega_b$  (close to  $\pi$ ). The point source response function of the antenna,  $G(\theta)$ , is normalized:  $G(0) = 1$ . The ratio of the power entering the system from the side lobe source at temperature  $T_B$  ( $h\nu \ll kT_B$ ) and emissivity  $\epsilon$ , to that from the universe at  $T_U$  is:

$$R = \frac{P_B}{P_U} = \frac{\epsilon_B B(\nu, T_B) \int_{\theta_0}^{\pi} 2\pi \sin \theta G(\theta) d\theta}{B(\nu, T_U) \Omega_s}$$

$$G(\theta > \theta_0) = \frac{B(\nu, T_U) \Omega_s}{\epsilon_B B(\nu, T_B) \Omega_B} R$$

$$G(\theta > \theta_0) = \frac{1.44 \nu}{\epsilon_B T_B} \left( \frac{1}{e^{1.44 \nu / T_U} - 1} \right) \frac{\Omega_s}{\Omega_B} R$$

Assume $\epsilon_B = 1$ ,	$T_B = 250^\circ K$ ,	$\theta_{BEAM} = 7^\circ \text{FWHM}$
$\Omega_B \approx \pi$	$T_U = 2.7^\circ K$	$\theta_0 = 85^\circ$

$$\Omega_s / \Omega_B = 3.7 \times 10^{-3}$$

The absolute precision of the measurement requires  $R < 10^{-3}$ .

Figure 2 shows the antenna point source response in db required for all angles larger than  $85^\circ$ . Plotted as well is the relative antenna gain,  $G(\theta > 85^\circ)$ , for the test horn extrapolated to other frequencies.

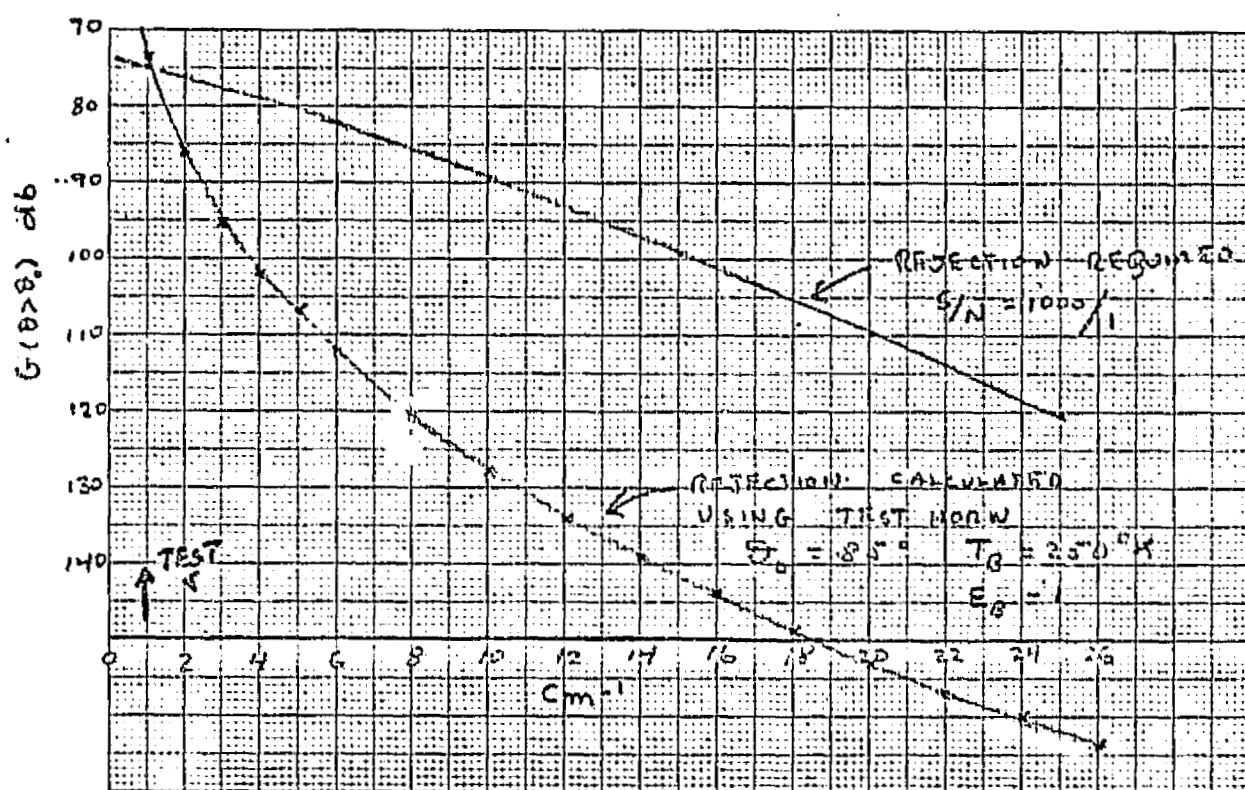


Figure 2

JET PROPULSION LABORATORY

INTEROFFICE MEMORANDUM

334-77-SMB

July 7, 1977

TO: M. Janssen  
FROM: S. Bednarczyk  
SUBJECT: Antenna Test

Antenna patterns of the Exponential Microwave Horn submitted by Dr. R. Weiss of M.I.T. were performed on June 24-27, 1977. These patterns consisted of measuring the relative power detected by the horn/detector (receiver) as a function of its angle to the wave front illuminating the horn. Patterns were taken in which the receiver cut the "E" as well as "H" planes of the transmitter wave. Cross-polarized and 45° plane cuts were also performed to give a better view of any asymmetry or misalignment in the horn. A set of patterns was also taken to confirm system linearity to within the specified tolerance of  $\pm 0.5\text{db}$ .

Antenna Range Configuration:

The JPL Mesa, south range at Building 212 was used. The range comprised of a test transmitter and the receiver, each mounted on individual antenna positioners approximately 20 feet above ground level (see Figure 2). These positioners were separated by  $\approx 54$  feet, a distance which was determined experimentally to give acceptable receiver sensitivity (noise level) as well as uniform illumination, within limitations of the range geometry.

In a typical run, the receiver antenna would be rolled about its symmetrical axis to align it with the arriving wave front from the transmitter according to the type of pattern desired (E, H, Cross, or 45° plane cut). The receiver is then rotated in azimuth  $\pm 180^\circ$  ( $\pm 90^\circ$  from the maximum power point).

Test Transmitter:

The test transmitter consists of a solid-state Gunn Oscillator with an output of  $\approx 10\text{mw}$  at a measured frequency of 31.32GHz into a standard 8° rectangular horn. The horn is also rotatable through  $90^\circ$  with respect to the horizontal plane so as to provide both "E" and "H" plane cuts. Calibrated attenuators were also included in order to check system linearity (see photo #1).

Test Receiver:

The receiver consisted of the M.I.T. Exponential horn with a crystal detector (HP-11517 with Ka Band rectangular waveguide adaptor). A rigid mount consisting of aluminum plate and rods was constructed to provide a stable platform. Adjustment screws near the base of the antenna were included to help boresight the antenna (see photos #2 and #3). The mount was wrapped with microwave absorber to minimize unwanted reflections and leakage entering the detector through any direction other than the antenna face.

Measurement System:

The Scientific-Atlanta series 1750 phase-locked receiver, crystal bolometer, and rectangular recorder were used to obtain the patterns.

The receiver locks to the transmitter signal by means of a harmonic generation system through use of an S-Band ( $\approx 3.9$  GHz) local oscillator and provides an IF output signal relative to the received signal strength.

Each of the patterns submitted contains information which describe the type of measurement its relation to others in the set, and are self-explanatory.

*Steve M. Bednarczyk by tab*  
Steve M. Bednarczyk

SMB:tab

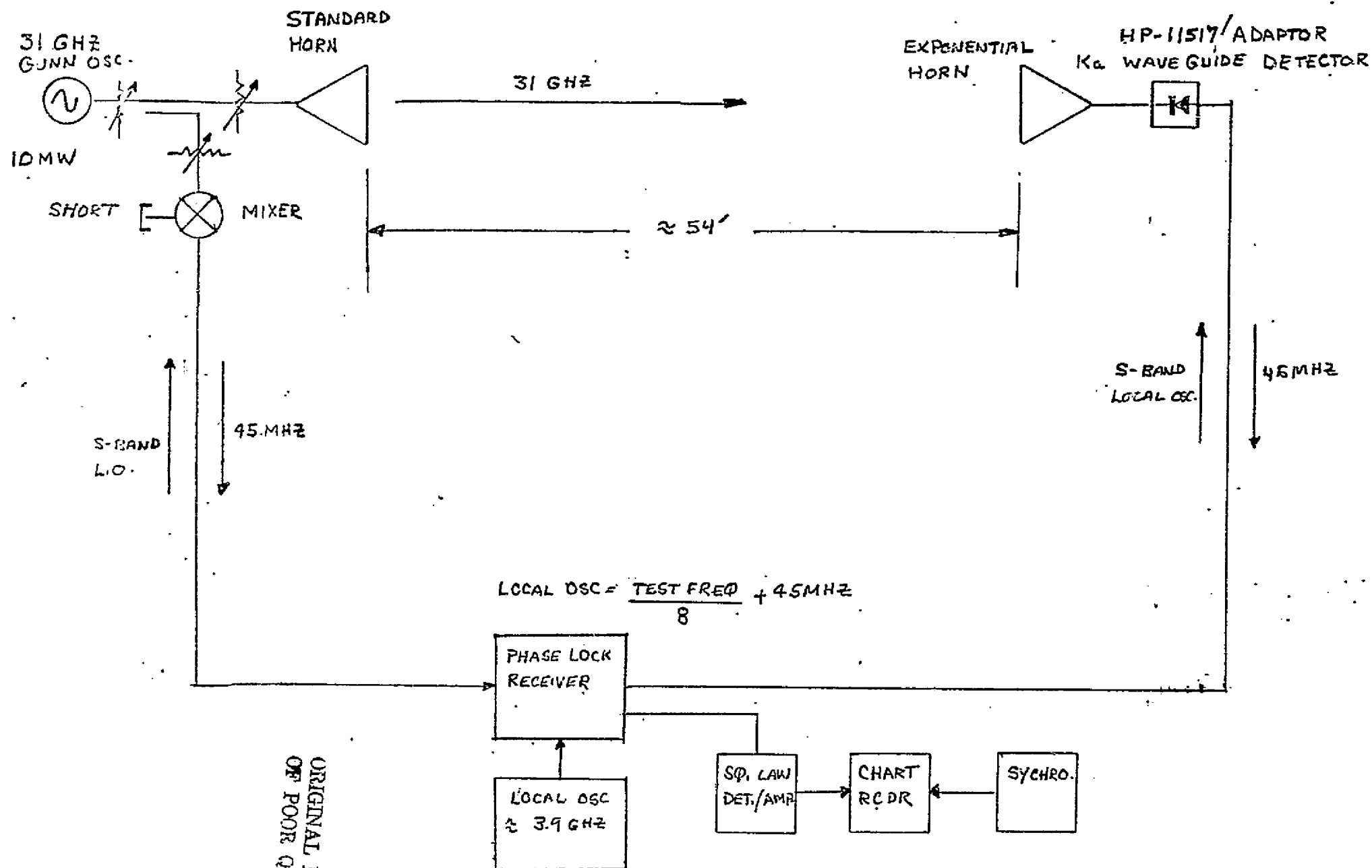
Attachments:

cc: H. Marlin  
N. Yamane  
R. Weiss



TRANSMITTER.

## RECEIVED

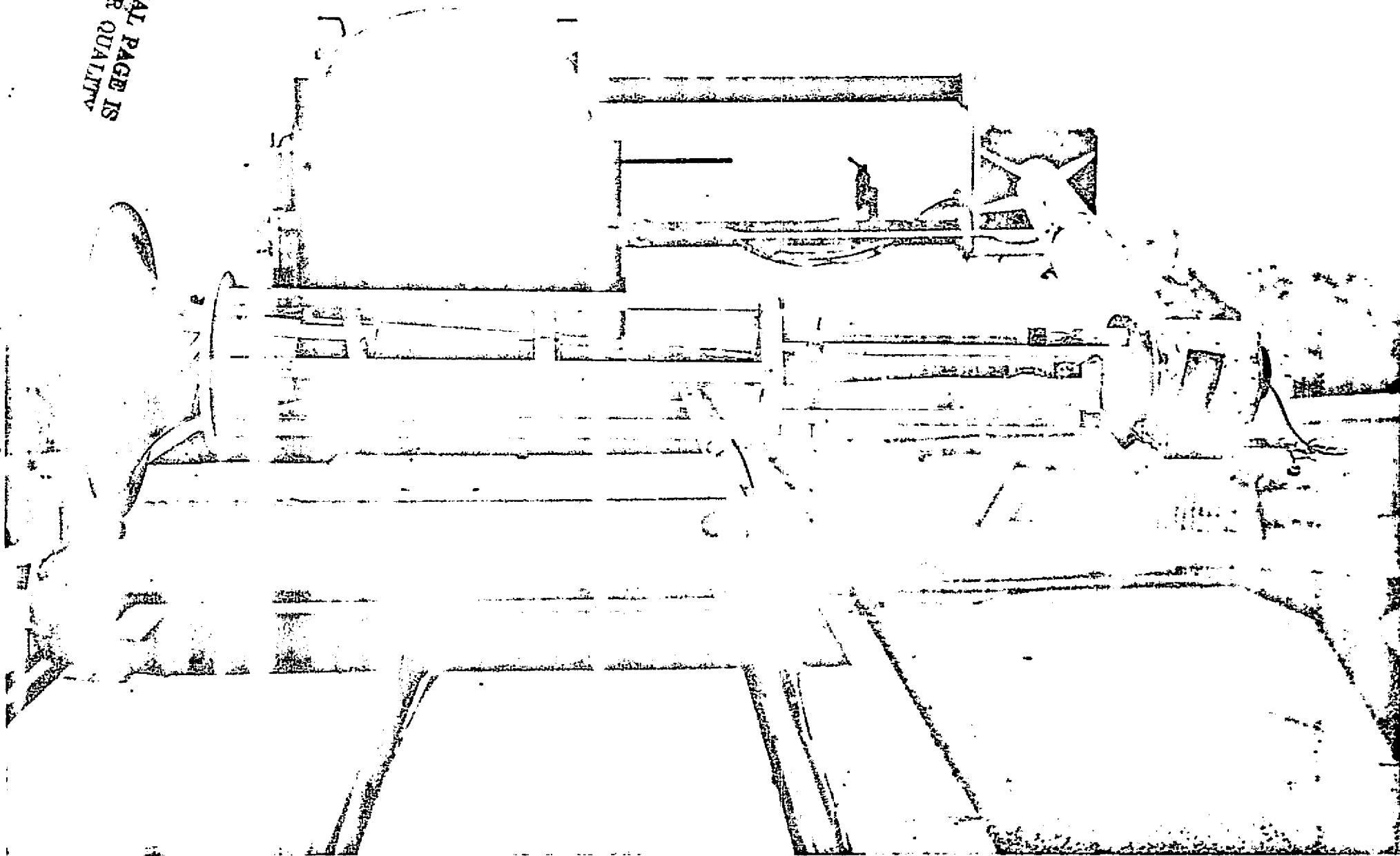


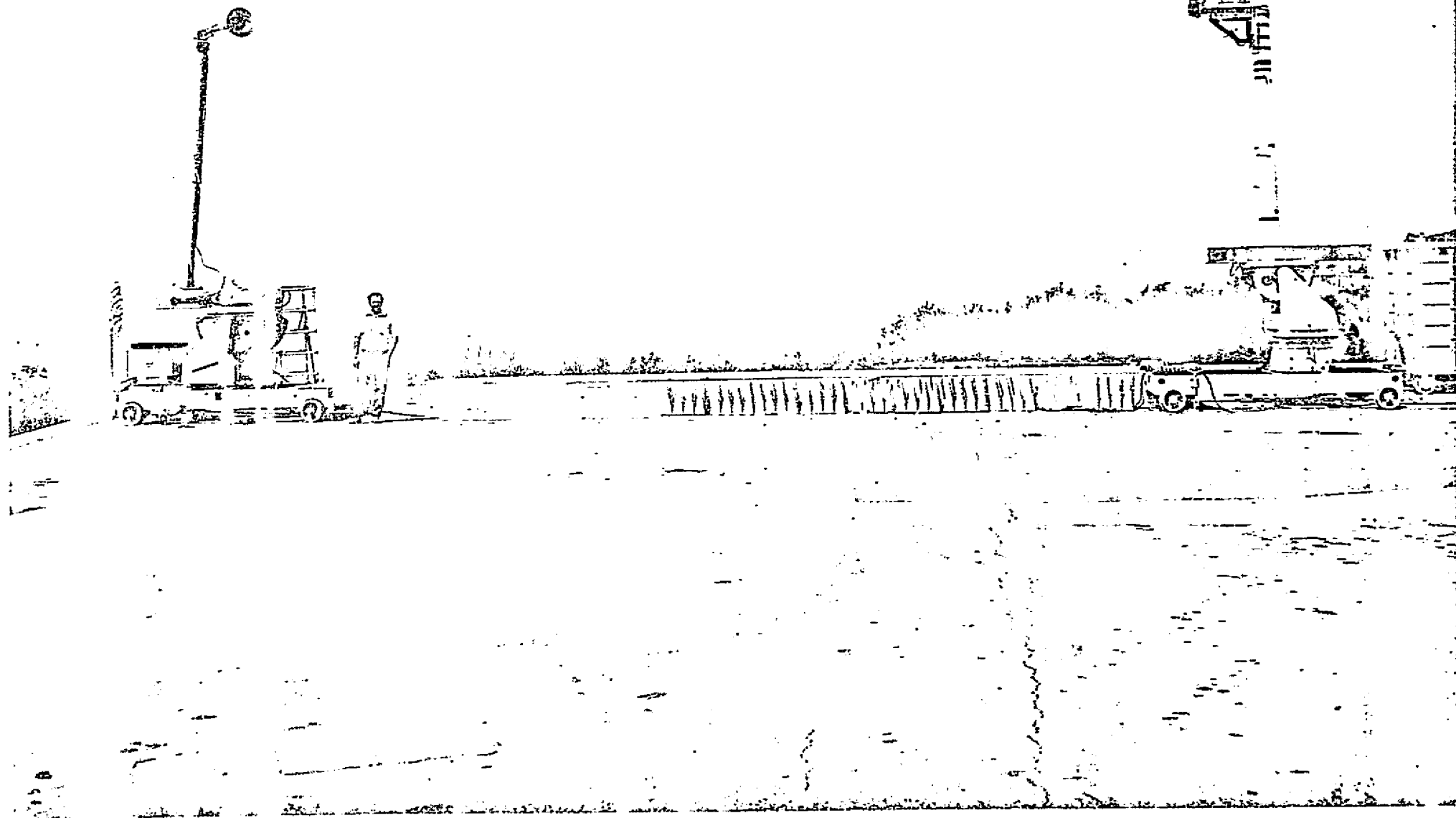
ORIGINAL PAGE IS  
OF POOR QUALITY

# TEST SYSTEM

FIGURE 1

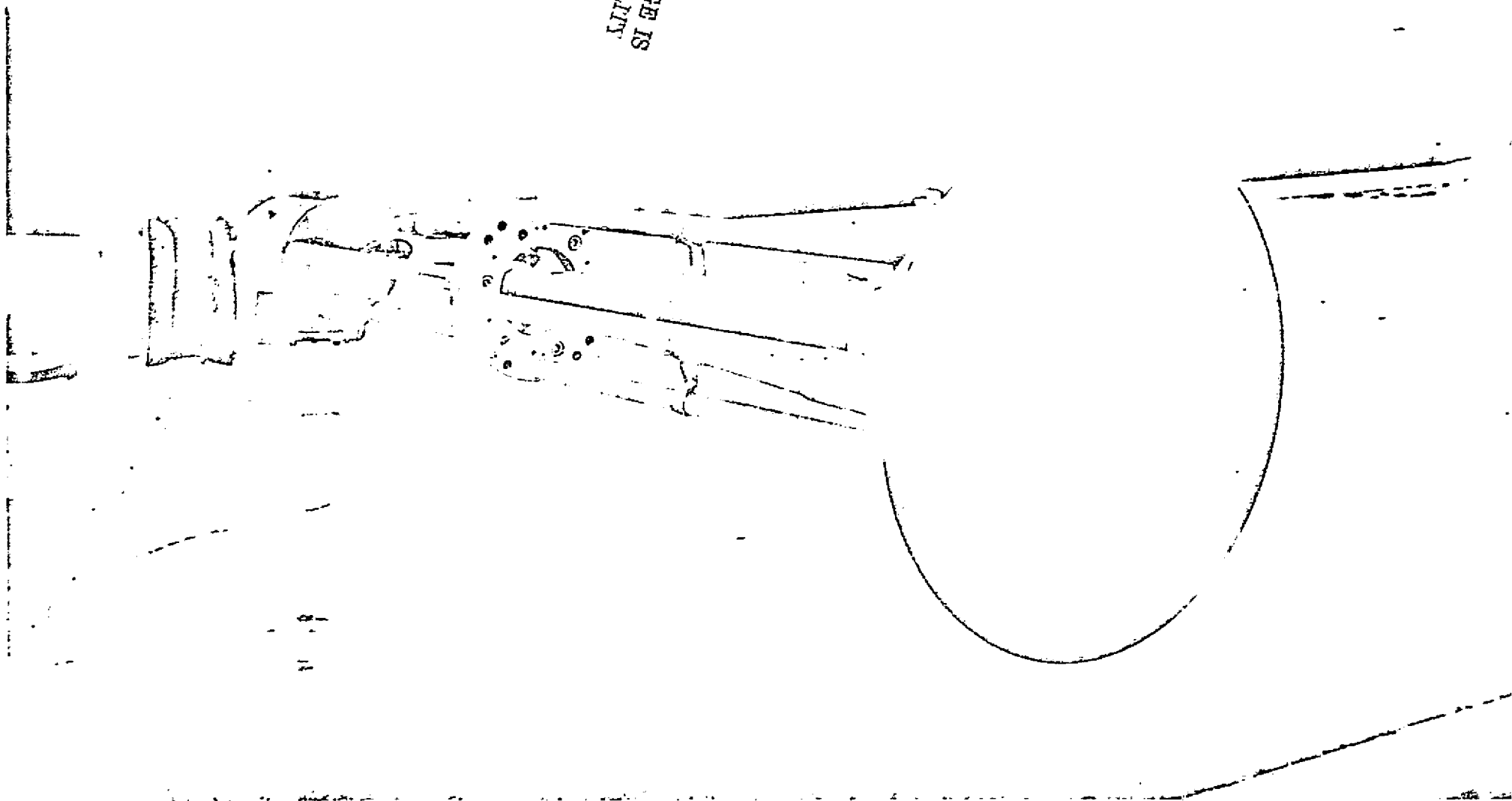
ORIGINAL PAGE IS  
OF POOR QUALITY



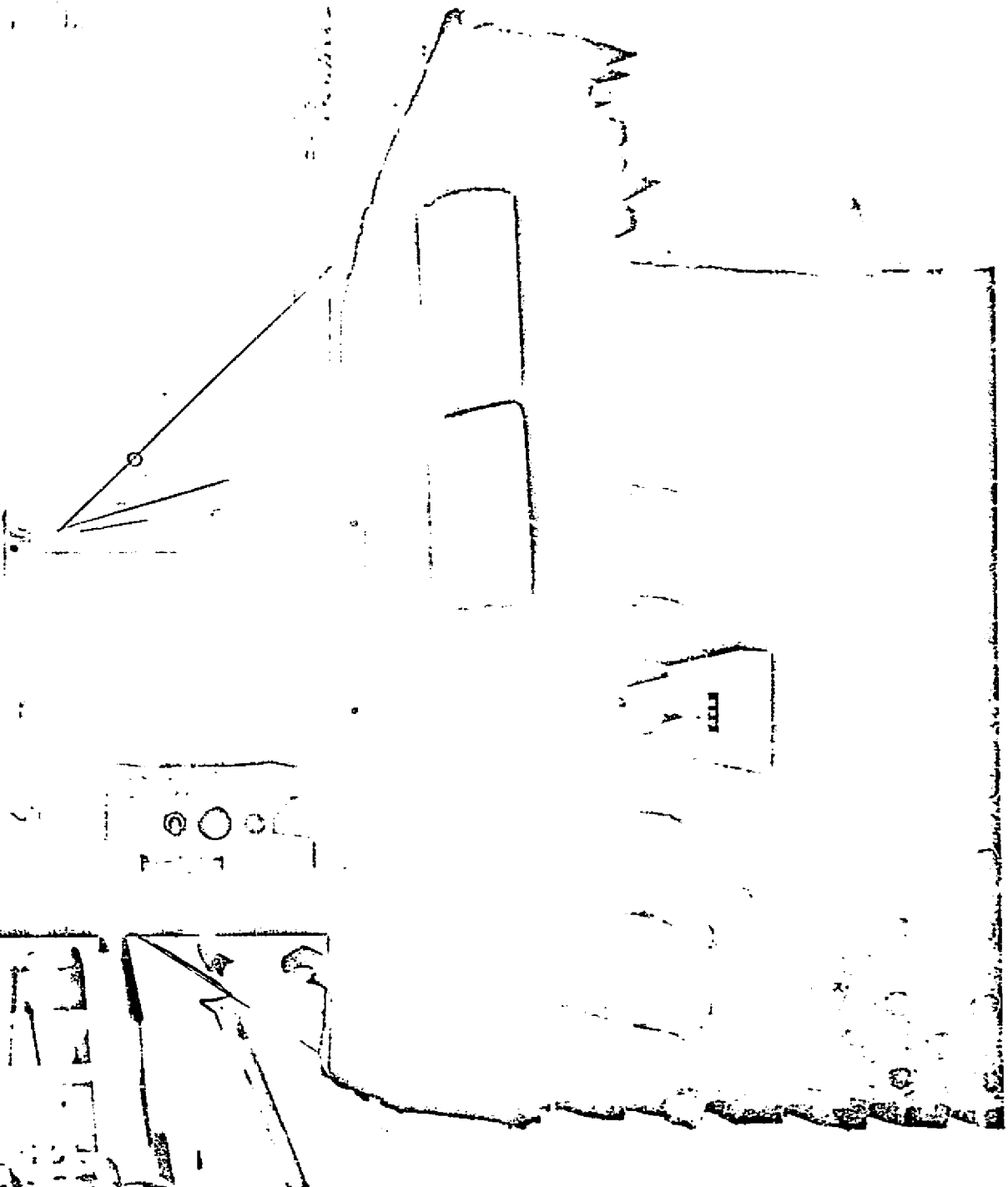


45

ORIGINAL PAGE IS  
OF POOR QUALITY



ORIGINAL PAGE IS  
OF POOR QUALITY



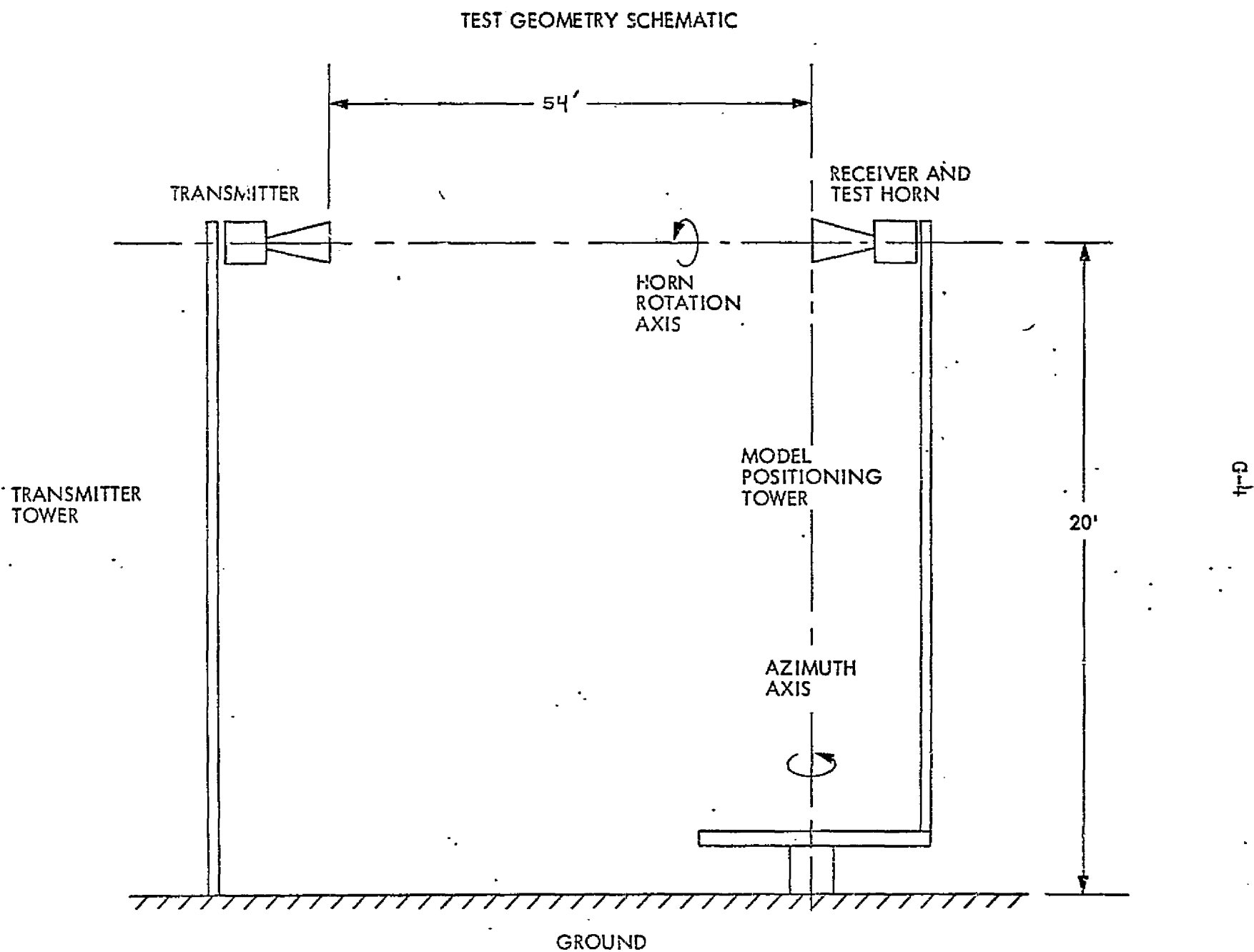


FIGURE 2

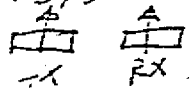
PATTERN NO. 3 DATE 6-27

PROJECT WEISS

ENGRS. S.M.B.

REMARKS 54 foot range.

HEAD: 340°



H-cut.

L.O.: 24 MHz

0 db RELATIVE POWER  
REFERENCE FOR ALL PATTERNS  
# 2 THEN #14

RELATIVE POWER ONE WAY - (db)

RELATIVE POWER ONE WAY - (db)

ORIGINAL PAGE IS  
OF POOR QUALITY

25  
30  
35  
40  
45  
50  
55  
60  
65  
70  
75  
80

25  
30  
35  
40  
45  
50  
55  
60  
65  
70  
75  
80

A

E

12

36

12

72

12

123

PATTERN NO. 4 DATE 6-27

PROJECT WEISS

ENGRS. S.M.B.

REMARKS H-cut

REF: 340°



RELATIVE POWER ONE WAY (dB)

REFLECTIONS FROM  
ADJACENT BUILDINGS

ANGLE

ZEROES OF  
AIRY FUNCTION

MAXIMA OF  
AIRY FUNCTION

KELLER THEORY  
 $E_{II}$

RELATIVE POWER ONE WAY (dB)

CHART NO. 121



PATTERN NO. 5 DATE 6-27

PROJECT WEISS

ENGES. S.M.B.

REMARKS H-cut

REF: 160°

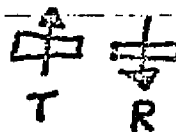


IMAGE OF #4

RELATIVE POWER ONE WAY (db)

25  
30  
35  
40  
45  
50  
55  
60  
65  
70  
75

ORIGINAL PAGE IS  
OF POOR QUALITY

ANGLE

RELATIVE POWER ONE WAY (db)

5  
10  
15  
20  
25  
30  
35  
40  
45  
50  
55  
60  
65  
70  
75  
80

CHART NO. 121-25

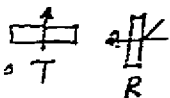
PATTERN NO. 6 DATE 6-27

PROJECT WEISS

ENGRS S.M.B.

REMARKS

HEAD  
REF: 250° T



CROSS-POLARIZED.

0 dB — GAIN REFERENCED TO  
PATTERN #3 (6-27-77)

RELATIVE POWER ONE WAY (dB)

RELATIVE POWER ONE WAY (dB)

BUILDINGS THIS  
SIDE

ANGLE

CHART NO 12172

PATTERN NO 7 DATE 6-27-77

PROJECT WEISS

ENCRS. S.M.A. (T) (R)

REMARKS

CROSS POLARIZATION  
IMAGE OF #6  
HEAD REF: 70°

RELATIVE POWER ONE WAY (dB)

RELATIVE POWER ONE WAY (dB)

ANGLE

CHART NO 37-42

BUILDINGS  
HERE

0 36 GAIN REF.

RELATIVE POWER ONE WAY (dB)

RELATIVE POWER ONE WAY (dB)

ANGLE

CHART NO 37-42

BUILDINGS  
HERE

0 36 GAIN REF.

PATTERN NO. 8 DATE 6-27

PROJECT WEISS

ENGRS S.M.B.

REMARKS



45°  
cut

HEAD  
REF: 250

RELATIVE POWER ONE WAY (db)

RELATIVE POWER ONE WAY (db)

ANGLE

CHART NO. 17-89

ORIGINAL PAGE IS  
OF POOR QUALITY

PATTERN NO. 9 DATE 6-27-72

PROJECT WEISS

ENGRS. S.M.B.

REMARKS

4  
(T) 45°  
(R)

IMAGE OF #8

RELATIVE POWER ONE WAY (db)

RELATIVE POWER ONE WAY (db)

ANGLE

CHART NO.

0 db GAIN REF

18°  
108

2  
12  
72

18°  
108

PATTERN NO. 10 DATE 6-27

PROJECT WEISS

ENGRS. S.M.B.

REMARKS



45°

HEAD REF: 2980

RELATIVE POWER ONE WAY (dB)

RELATIVE POWER ONE WAY (dB)

ANGLE

ORIGINAL PAGE IS  
OF POOR QUALITY

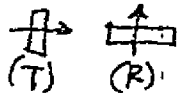
PRINTED IN U.S.A.

PATTERN NO. 11 DATE 6-27

PROJECT WEISS

ENGRS. S.M.B.

REMARKS



REF: 340°

RELATIVE POWER ONE WAY (db)

RELATIVE POWER ONE WAY (db)

BUILDINGS ON THIS  
SIDE

ANGLE

CHART NO. 121-90

CHART NO.

PATTERN NO. 12 DATE 6-27-77

PROJECT WEISS

ENCRS. S.M.B.

REMARKS

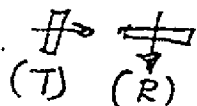


IMAGE OF #11

HEAD REF: 160°

RELATIVE POWER ONE WAY (db)

RELATIVE POWER ONE WAY (db)

ANGLE

ORIGINAL PAGE IS  
OF POOR QUALITY

NOISE FROM  
EVENT MARKER  
INADVERTENTLY PUSHED

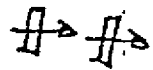


PATTERN NO. 13 DATE 6-21-73

PROJECT WEISS

ENGRS. S.M.R.

REMARKS E-CUT



HEAD REF: 76°

RELATIVE POWER ONE WAY (db)

RELATIVE POWER ONE WAY (db)

0 db GAIN REF.

ANGLE

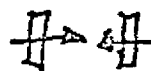
CHART NO. 2700

PATTERN NO. 14 DATE 6-27

PROJECT WEISS

ENGRS. S.M.B.

REMARKS



HEAD: 250°

IMAGE OF #13

RELATIVE POWER ONE WAY (dB)

RELATIVE POWER ONE WAY (dB)

ANGLE

CHART NO. 12110

0db  
↓ GP ↓ P ↓ F ↓  
ZEROS OF  
AIRY FUNCTION

MAXIMA OF  
AIRY FUNCTION

KELLER  
THEORY

$\epsilon_1$

RELATIVE POWER ONE WAY (dB)

RELATIVE POWER ONE WAY (dB)

ANGLE

CHART NO. 12110

# COBE STUDY

## NOISE-RESOLUTION TRADE OFF

We take the basic equation:

$$\frac{S}{N} = \epsilon B_{\nu}(T) \Delta\nu A\Omega \sqrt{T_{\text{int}}} / \text{NEP}$$

with:  $A\Omega = 0.5 \text{ cm}^2 - \text{sr}$

$$\epsilon = 0.1$$

$$\text{NEP} = 3 \times 10^{-14} \text{ w}/\sqrt{\text{Hz}}$$

$$T_{\text{int}} = 3 \times 10^4 \text{ seconds} \quad (1 \text{ yr over } 10^3 \text{ beams})$$

and obtain:

$$N = \left(\frac{1}{\Delta\nu}\right) 3.4 \times 10^{-15} \text{ w/cm}^2/\text{cm}^{-1}/\text{sr}$$

This is greater than  $10^{-3}$  of the peak BB flux for  $\Delta\nu \leq \frac{1}{4}$ .

For  $\Delta\nu > \frac{1}{4}$ , we are limited by the calibration uncertainty of 1 part per thousand, while for  $\Delta\nu < \frac{1}{4}$ , we are limited by detector noise. I have computed some model fits to assumed data, using the above noise or  $10^{-3}$  of the peak flux, whichever is greater. These results apply to five parameter fits of the form:

$$I_{\nu}(\text{obs}) = K_{\nu}(T_c, \gamma) + \tau_0 \left(\frac{\nu}{\nu_0}\right)^{\alpha} B_{\nu}(T_d)$$

where  $K_{\nu}$  is the solution to the Kompaneets equation and the second term represents galactic dust. Using only the 0-20  $\text{cm}^{-1}$  data, I find substantial

correlation among the parameters ( $\rho_{yT_c} \sim 0.9$ ), but fits are still possible. The following figure shows 95% confidence intervals on  $y$  and  $T_c$  as a function of resolution.

The following points should be made:

- 1) Better detectors (or higher  $\epsilon$ ) shift the optimum  $\Delta v$  to smaller values.
- 2) Better calibration shifts  $\Delta v_{opt}$  to higher values.
- 3) Correlated calibration errors produce a broad, flat optimum.

E. Wright

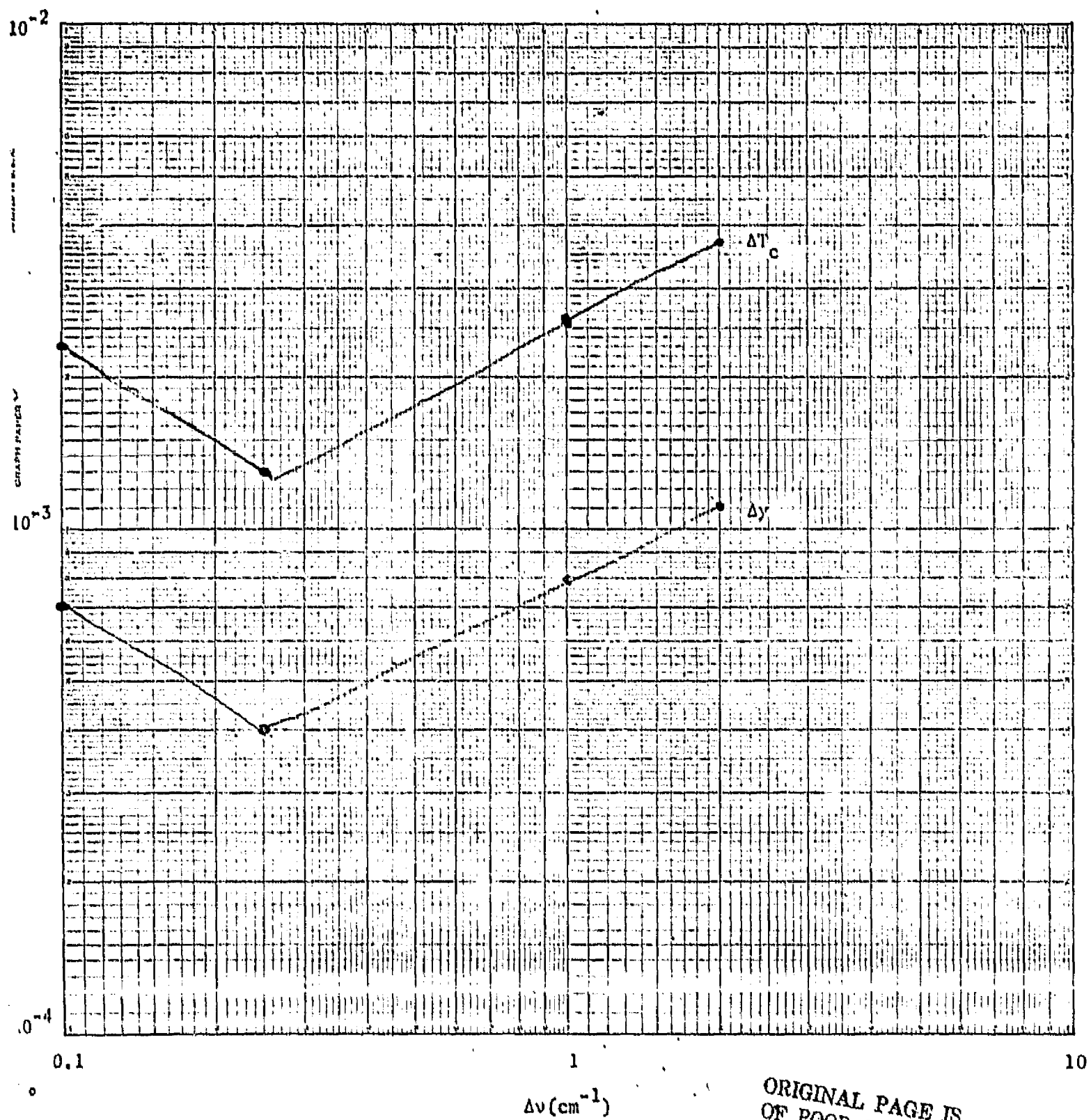


Figure 2: 95% Confidence Intervals on  $T_c$  and  $y$  vs. Resolution

## PRELIMINARY FINDINGS ON FLEXURE HINGES

A Bendix Flexpivot, model #5016-800, was acquired and hysteresis losses and off-axis displacement were measured.

The off-axis displacement was checked using a laser beam reflected from a mirror positioned over the axis of rotation. We found for an angle of rotation of  $15^\circ$  there was an off-axis displacement of  $10'$  of arc. This test was performed at  $300^\circ\text{K}$ .

The hysteresis losses were checked using an auto-collimator and a mirror mounted over the rotation axis.

At  $300^\circ\text{K}$ , the following results were obtained:

<u>Angle of Rotation</u>	<u>Hysteresis Angle</u>
0	"0"
<u><math>+10^\circ</math></u>	$1.5'$
<u><math>+15^\circ</math></u>	$3.75'$
<u><math>+20^\circ</math></u>	$9'$

These results were consistent with the manufacturer's specifications, although slightly above average.

At  $77^\circ\text{K}$ , though, the following hysteresis angles occurred:

<u>Angle of Rotation</u>	<u>Hysteresis Angle</u>
0	"0"
<u><math>+10^\circ</math></u>	$8'-10'$
<u><math>+15^\circ</math></u>	$23'$
<u><math>+20^\circ</math></u>	$>30'$

At  $77^\circ\text{K}$ , the pivot had taken a different rest position than at  $300^\circ\text{K}$  by  $\approx 30'$ .

The power that is dissipated for a given hysteresis angle can be found by using the formula:

$$P = \frac{2(\Delta \theta)^2 K \times 10^{-7}}{t} \text{ Watts}$$

where  $\Delta \theta$  is the hysteresis angle in radians, K is the torsional spring rate in dyne-cm/rad and t is the period.

Two attempts were made to construct a linear transport mount using torsional springs.

The first one was made using springs machined from .005" Be-Cu stock (see Fig. 1). The two springs were soldered to the ends of a brass tube and a rod suspended between them. Several problems emerged from this attempt:

- (1) The springs themselves were not initially flat.
- (2) The plane of the hinges was not parallel.
- (3) The rod was not centered.

All three problems gave large off-axis displacements of anywhere from 30' to 1° or 2°.

A second approach was tried using individual arcs as springs (see Fig. 2). The problems associated with this design are the following:

- (1) The plane of the springs has to be the same.
- (2) The arc length of each side of the spring has to be equal between the clamps.
- (3) The centering of the rod.

A line-up jig was devised to ensure as far as possible the minimization of the above problems.

A loudspeaker movement was used to drive the mount and a capacitive bridge to determine the position.

The off-axis displacement was checked first and for the maximum travel end to end ( $\approx 1$  cm) amounted to 2' of arc. This was a very strong



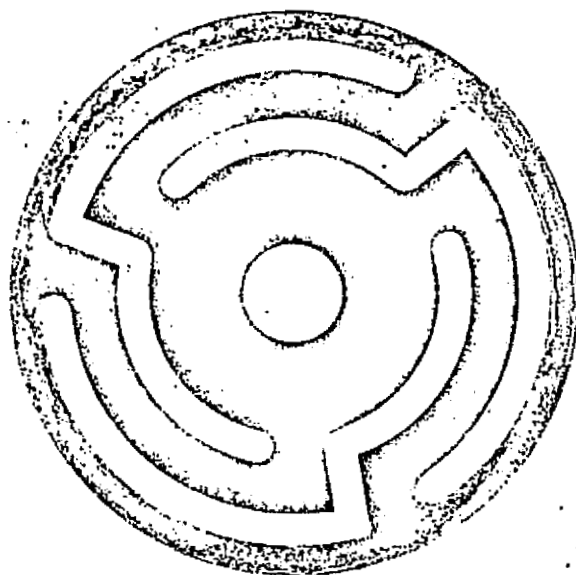
function of the assembly procedure--the first attempts having large deflections ( $\approx 20'$  of arc). After some practice, it was reduced to the  $2'$  of arc.

The spring characteristics were checked by driving the loudspeaker coil (DC) and reading the capacitance bridge for the position.

Figure 3 is a plot of the position as a function of voltage. On the "+" voltage side, there is a "dip" in the curve. This appears to be caused by one spring not being aligned in a flat plane and buckling occurs when this position is reached.

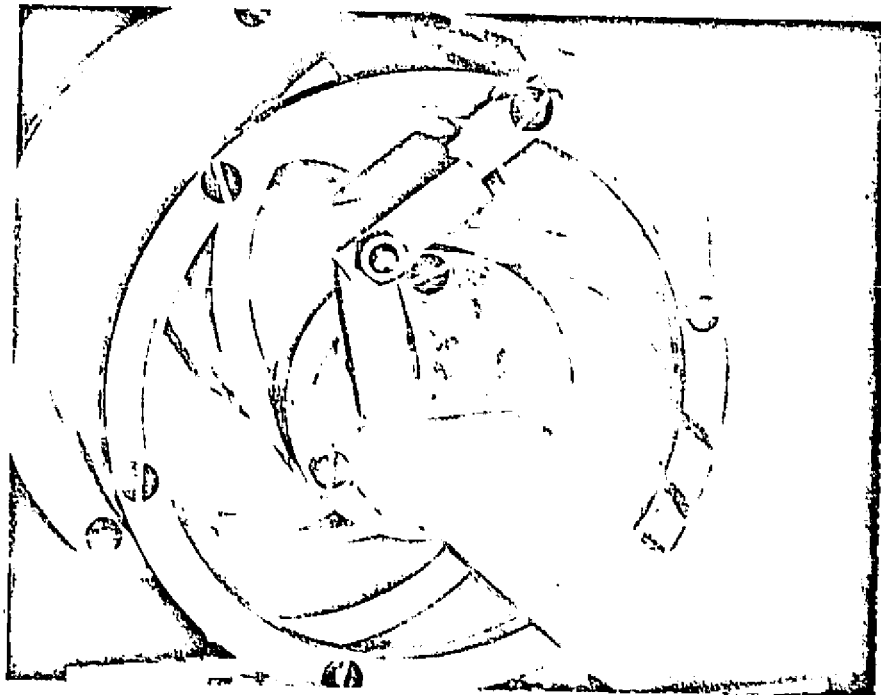
Figure 4 is a calibration of the capacitance bridge using a micrometer to position the mount.

Richard Benford



ORIGINAL PAGE IS  
OF POOR QUALITY

FIGURE 1



ORIGINAL PAGE IS  
OF POOR QUALITY

FIGURE 2



### FIGURE 3

27/2/78

Plot of Capacitor displacement  
vs. micrometer position.

NAR reading 5mV scale.

5

4

3

2

1

0

.01

.02

.03

.04

.05

Micrometer reading (inches)

ORIGINAL PAGE IS  
OF POOR QUALITY

BIMONTHLY REPORT  
INTERFEROMETER DESIGN AND CONSTRUCTION

FIRAS Mock-Up Design

We have chosen the symmetrized Martin-Puplett optical path, using mirrors that are available from Special Optics. The basic path is:

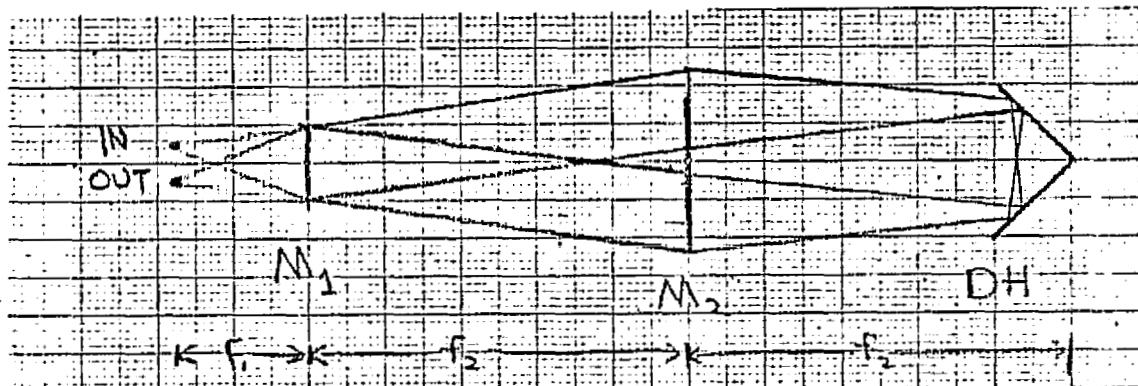


Figure 1

$M_1$  is a parabola, used  $43^\circ$  off axis, with FL = 14 cm and diameter = 13 cm, while  $M_2$  is also a parabola, used  $29^\circ$  off axis, with FL = 40 cm and size 23 x 20 cm.

Ideally,  $M_1$  should have a longer focal length but Special Optics couldn't make it, and other sources would cost ~ \$10K more.

In Figure 2, a top view of the device, the inputs and outputs are located over the  $M_1$ 's which collimate the light and redirect it horizontally to  $M_2$  which produces an image of the input-output pair on the dihedral. At the dihedral, the input beam is switched from low to high and returned through  $M_2$  and  $M_1$  becoming the output.

The input-output polarizer, IP-OP, and the beamsplitter, BS, are both wire grid polarizers, but are oriented as follows: the IP-OP is vertical, while the BS is cocked at  $45^\circ$  to vertical, so the polarizations are mixed, leading to interference.

#### Other Designs Considered

Before settling on the symmetrized MP interferometer, we also considered the symmetrical Mach-Zender system (the Block Engineering concept) and the assymmetric MP in the COBE Phase A study.

Because the NZ uses skew beams in the interferometer, the  $f\#$  must be high, which requires a large retroreflector. In effect, the retroreflector must be as wide as the dihedral in the symmetrized MP system is high. This leads to a larger system without any compensating advantages.

The ordinary MP interferometer is quite compact and the input and outputs are well separated. It wastes one polarization, however, and it is polarization sensitive, and it doesn't treat the sky horn and the internal calibrator exactly alike. Once the symmetrized MP seemed feasible, we abandoned the assymmetric MP.

#### Transport

The mirror motion needed to vary the path difference is obtained by moving both dihedrals parallel to the  $M_2-M_2$  line. Moving both dihedrals by  $X$  cm changes the relative delay by  $4(\cos\theta)X$  where  $\theta$  is  $29^\circ$ , the off-axis angle at  $M_2$ . In order to obtain 5 cm delay (for  $.1 \text{ cm}^{-1}$  unapodized resolution), the total stroke is  $X \approx 1.43$  cm. During this motion the beams move by  $X\sin\theta = .70$  cm on the dihedral, so the mirrors must be this much oversized.

The solid angle of the beam at the transport must be  $\Omega \leq \frac{2\pi\Delta\nu}{\nu}$ . We have designed to  $(\nu/\Delta\nu) \leq 200$ , so  $\Omega < \frac{\pi}{100}$ , corresponding to an f/5 beam. For a throughput of  $0.5 \text{ cm}^2\text{-sr}$ , the area of the beam gives a diameter of 4.5 cm, so the extra 0.7 cm is a small penalty.

### Diffraction

Consider a focused beam with intensity given by:

$$I \sim \left[ \frac{2J_1(X)}{X} \right]^2, \quad X = \frac{\pi r}{\lambda(f\#)}$$

The second dark ring of this pattern occurs at  $X = 7$ , giving  $r = 2.23 \lambda(f\#)$ . We have chosen  $X = 7$  at  $\lambda = 1 \text{ mm}$  as our design limit, and tried to size the mirrors to allow a skirt of width  $0.223(f\#)$  cm around the geometric spot. But the diameter of the geometric spot is determined by the throughput  $\Delta\Omega$  and the f#, giving  $r_{\text{geo}} = .45(f\#)$ . Thus our design criterion translates into allowing a 50% margin on the mirrors. At the dihedral, where the geometric spot is 4.5 cm, we allow 6.75 cm.

At  $M_2$  where the beams are not focussed, the situation is slightly more complicated. We take  $40/4.5 = 8.9$  as the f#, so the required margin is 2 cm. The geometric spot size is  $4.5 + 40/5 = 12.5 \text{ cm}$ , so the required diameter is 16.5 cm. Due to the tilt of  $M_2$ , the true width is 18.9 cm, and due to the separation of input and output on  $M_2$ , the height is 23.25 cm.

At  $M_1$ , we need a mirror 13.66 cm in diameter, or  $13.7 \times 19.3$  because of the tilt, in order to include our diffraction criterion. However, we do not want diffracted rays reflected from the Winston cones at the input and output to form cavity resonances. Thus we will probably place an absorbing stop at  $M_1$  just beyond the geometric beam.



### Ray Tracing

We have developed a ray-tracing program for our PDP11 that is designed for off-axis systems, rather than axial ones. This program can handle flats, dihedrals, trihedrals, spheres, ellipsoids, paraboloids and toroids.

With the focus of  $M_1$  between the input and the output, and the focus of  $M_2$  in the center of the dihedral, the system is perfect on axis, but off-axis aberrations are large but tolerable. Following a suggestion by John Mather, we found that the off-axis aberrations were improved by placing the focus of  $M_2$  in the center of  $M_1$ . Even better performance can be achieved by allowing arbitrary shapes for  $M_1$  and  $M_2$ , but the use of parabolas is adequate. Figure 4 shows some spot diagrams with the foci of  $M_2$  either in the center of  $M_1$ , or the center of the dihedral. Two cases are given for two different off-axis angles at  $M_1$ . We see that reducing the angle at  $M_1$  does not make a dramatic improvement, probably because the plane defined by input- $M_1$ - $M_2$  is perpendicular to  $M_1$ - $M_2$ -DH plane, so some aberrations cancel.

### Input-Output Optics

The current design gives an input diameter of  $(14/40) \times$  the diameter at the retroflector, or 1.6 cm, with an  $f\#$  of 1.75. The output is identical. We will use Winston cones to concentrate the output to a diameter of 4.5 mm.

As can be seen in Figure 3, the output beam is very convergent, making it difficult to insert a dichroic filter before the focal plane. Figure 3 shows a possible solution, with the dichroic filter at the focal plane, and refocussing optics behind it. However, the indicated scheme has intolerable aberrations when we ray trace it. Crossed off-axis paraboloids can be used, but the final design is not set. Changing the focal length of  $M_1$  to 20 cm increases the

available space to the point where the dichroic can be placed before the focal plane.

#### Progress in Orders

We have ordered the mirrors  $M_1$  and  $M_2$  from Special Optics and Winston cones from A. J. Tuck and Co. These parts should arrive in late July. We are designing mirror mounts so we can assemble the system on a lab bench for alignment, diffraction and resolution tests.

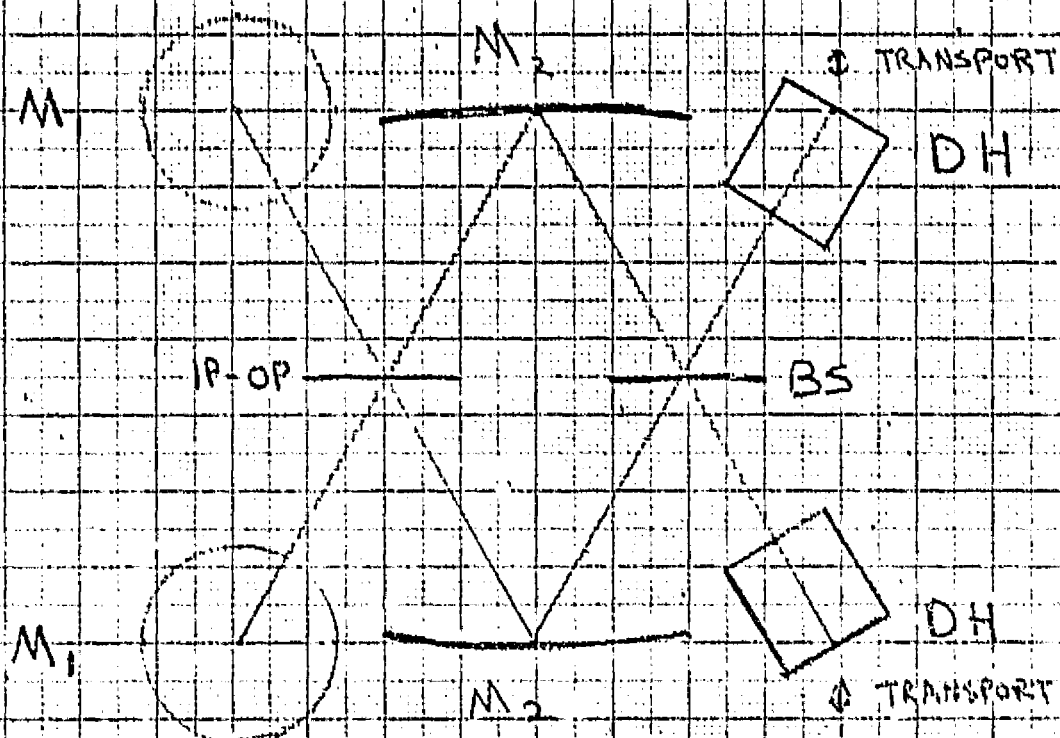


FIGURE 2: TOP VIEW OF INTERFEROMETER

ORIGINAL PAGE IS  
OF POOR QUALITY

40 1310

KOE 10 X 10 TO THE CENTIMETER 12 1 004  
KOEFFEL & ESSEPP CO. WMA WBSA

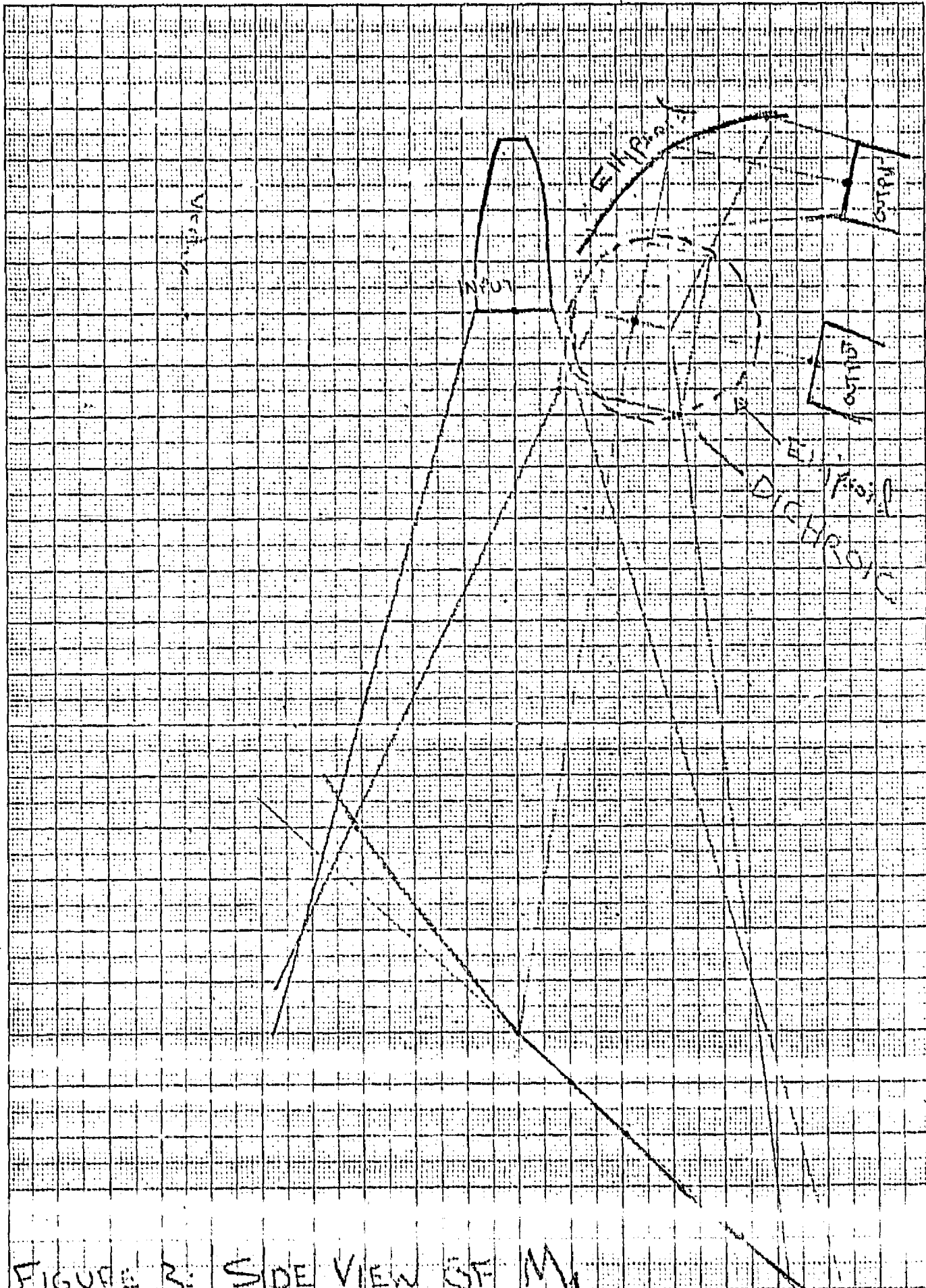


FIGURE B: SIDE VIEW OF M<sub>1</sub>

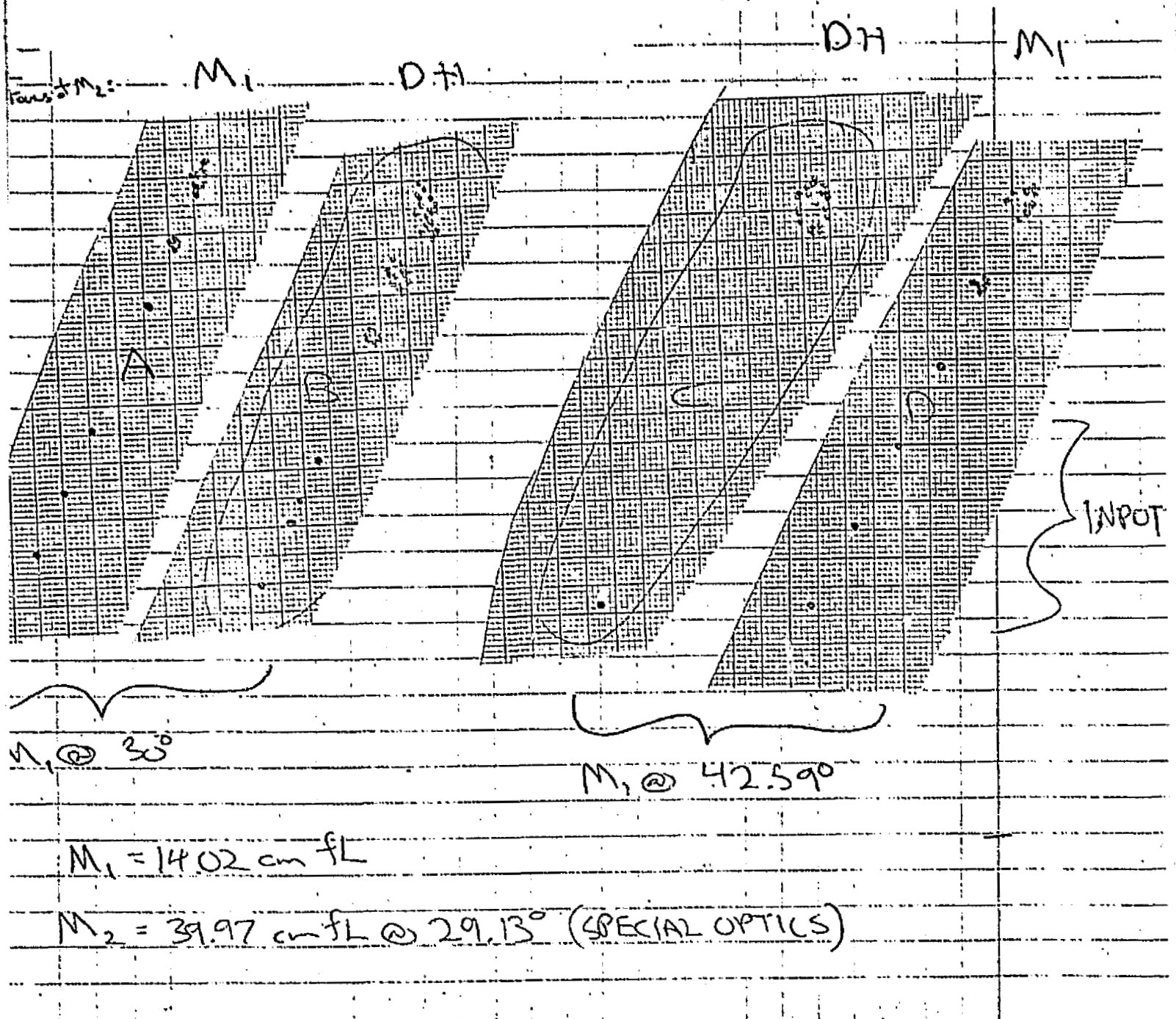


Figure 4: Each diagram shows inputs in the lower left and outputs in the upper right.

- A)  $M_1$  at  $30^\circ$ . Focus of  $M_2$  at  $M_1$ .
- B)  $M_1$  at  $30^\circ$ . Focus of  $M_2$  at DH.
- C)  $M_1$  at  $42.59^\circ$ . Focus of  $M_2$  at DH.
- D)  $M_1$  at  $42.59^\circ$ . Focus of  $M_2$  at  $M_1$ .

ORIGINAL PAGE IS  
OF POOR QUALITY

## Radiation Absorption by Thin Bismuth Films

### Introduction

Recently, several varieties of bolometers have been made for use in the detection of submillimeter radiation which employ thin metal films as absorptive elements<sup>1,2</sup>. These films, deposited onto a dielectric substrate, can have a negligible heat capacity and still absorb one half or more of the radiation in a single pass. An idealized thin metal film is completely described by its impedance but an actual vacuum deposited film might be somewhat more complicated. Thinly connected clumps of metal would act as a non-absorptive beam splitter, while a resistive film with stray conductive paths through it would absorb more radiation than its DC impedance would indicate. Therefore, measurements were made of the reflection and transmission of millimeter wavelength radiation by various resistive Bismuth films on Sapphire and Silicon substrates to deduce the absorption of radiation by these films as a function of DC impedance.

### Theory

In the standard waveguide analogy, one can calculate the admittance at the front surface of a dielectric wafer which has a resistive coating on its back surface as<sup>3</sup>

$$Y = n \left\{ \frac{\cos \theta'}{\sec \theta'} \right\} \left[ \frac{\left( Y_0 \left\{ \frac{\cos \theta}{\sec \theta} \right\} + \frac{1}{R_f} \right) \cos \beta d + i n \left\{ \frac{\cos \theta'}{\sec \theta'} \right\} \sin \beta d}{n \left\{ \frac{\cos \theta'}{\sec \theta'} \right\} \cos \beta d + i \left( Y_0 \left\{ \frac{\cos \theta}{\sec \theta} \right\} + \frac{1}{R_f} \right) \sin \beta d} \right] \quad \begin{cases} \text{for } E_{\perp} \\ \text{for } E_{\parallel} \end{cases}$$

where  $n$  is the index of refraction of the dielectric,  $\theta$  is the angle of incidence and  $\theta'$  the angle formed by the light to the normal inside the wafer,  $\nu$  is the frequency in wave numbers ( $\text{cm}^{-1}$ ),  $R_f$  is the film impedance,

d is the thickness of the wafer and  $Y = 1/377\Omega$  is the admittance of free space. The propagation constant inside the dielectric is

$$\beta = 2\pi nvd \cos\theta'$$

From the admittance we can obtain the reflectivity:

$$\rho = \frac{Y_0 \left\{ \frac{\cos\theta}{\sec\theta} \right\} - Y}{Y_0 \left\{ \frac{\cos\theta}{\sec\theta} \right\} + Y} \quad \begin{cases} \text{for } E_{\perp} \\ \text{for } E_{\parallel} \end{cases}$$

and the reflection, absorption and transmission coefficients are given by

$$R = \rho\rho^*, \quad A = \frac{(1-R)}{\left(1 + \frac{R_f}{377 \Omega/\square}\right)}, \quad T = 1-R-A$$

These expressions all exhibit a channel spectrum due to the frequency dependance of Y. This dependance vanishes when the load admittance matches the intrinsic admittance of the substrate. Thus one could make a spectrally flat absorber by choosing a film impedance such that

$$R_f = 377/(n-1).$$

To obtain theoretical predictions for the amounts of reflection from and transmission through each of our samples, the expressions given above were evaluated for an incident angle of  $45^\circ$  and averaged over the spectral response of our InSb "hot electron bolometers". There was a possible polarization of the incident radiation of as much as 3%, and there was some uncertainty as to the thickness of each sample and both of these showed up as uncertainties in the theoretical predictions for

specific samples. Figure 1 is a graph of reflection transmission and absorption calculated for films deposited on the back of a 15 micron thick piece of Silicon with an incident thermal spectrum [ $I(\nu) \propto \nu^2$ ] low pass filtered at  $14 \text{ cm}^{-1}$  plotted versus film impedance.

If the resistive coating is deposited onto the incident instead of the back surface there could be no impedance matching and thus there will always be a channel spectrum. Further, the frequency averaged absorption is very much reduced, as was verified in measurements of the Sapphire samples.

#### Measurements

Resistive layers of Bismuth were vacuum deposited onto thin wafers of either Sapphire or Silicon. The film impedances were measured at DC and the coated samples were cooled to  $4.2^\circ\text{K}$  and exposed to Submillimeter thermal radiation. The light reflected by them was measured by one InSb hot electron bolometer and that transmitted through them by another. These detectors had a pass band extending from  $1/2$  wave number to either 14 or 35 wave numbers, depending on whether or not low pass interference filters were used. Bismuth was chosen for the resistive layer because its high resistivity allows one to deposit a layer which is simultaneously thick enough to be spatially uniform and resistive enough to absorb radiation.

The Sapphire wafers used were between 30 and 50 microns thick, polished on both sides. The extraordinary optical axis lay nearly in the plane of each wafer. The Silicon samples were polished on one side and then etched on the other side to a thickness between 10 and 25 microns. The Bismuth was deposited on the etched surface. In separate depositions for the different crystals, wafers were held in a vacuum chamber at various distances from a Bismuth source to give a range of film impedances among the prepared samples. Glass slides with electrical leads attached were put



next to each sample to monitor the DC impedance during and after the deposition. To check the sensitivity of film impedance to the structure of the surface it is deposited onto, large wafers of Silicon with the same surface treatment as the smaller samples were included in the evaporation onto Silicon along with the glass slides as additional DC monitors. Evaporations took place in a background pressure of less than  $2 \times 10^{-6}$  torr.

It was found that the Bismuth films changed in impedance due to hydrolization in the atmosphere, especially as water condensed on them when they were removed from cryogenic liquids. To inhibit this a thin layer of SiO was deposited on the samples during the same evaporation as the Bismuth. With this protective coating the film impedances have not changed noticeably in over one year of exposure to the atmosphere and numerous cyclings to liquid Helium temperatures.

Judging from the weight of Bismuth evaporated, the films have a resistivity of roughly  $4 \times 10^{-4}$  ohm-cm at room temperature, or four times the bulk value. The film impedances increase by a factor of roughly 1.6 as they are cooled to 4.2°K and are then constant down to 1.2°K, the lowest temperature at which they were measured. At liquid Helium temperatures the films deposited onto Silicon substrates have impedances which are higher than the impedances of the corresponding glass slides (+9%, [-4%]) and the DC impedances measured on Silicon agree to within error with the best fit of measurements to calculation for the impedances seen by the radiation field at a frequency of several hundred gigahertz.

The prepared samples were mounted, coated surfaces down, at 45° to the incident radiation and immersed in liquid Helium along with the two detectors. Reflection and transmission were measured for each of eight coated samples, a blank wafer of each kind of crystal, a gold mirror and

the brass holder when emptied of samples. After subtraction of the background reflection due to the holder, the reflection from each sample was normalized to the reflection from the gold mirror. The transmission through each sample was normalized to the transmission through the empty holder.

### Results

When the highest frequency in the input spectrum was limited to  $14\text{cm.}^{-1}$ , the measured reflection and transmission coefficients for the coated and the blank samples agreed with the theoretical predictions to within about 2%. However, when the pass band was allowed to extend to the  $35\text{cm.}^{-1}$  cutoff of cold fluorogold the data for reflection lie systematically below the expected values by about 5% of the full intensity of the incident light, while the transmission data are again in fairly good agreement with theory. It is striking that the deficit in reflection at high frequencies seems to be a constant, independent of the amount of reflection, the film impedance, the choice of substrate material and perhaps even the presence or absence of any coating at all on the sample. See Figure 2 and 3.

This slight deficit in the high frequency reflection is most likely due to systematic measurement errors. The reflection measurements were much more sensitive to the geometry of the apparatus and it is not likely that the uncoated samples would show the same discrepancy due only to random errors. It was therefore deemed not worthwhile to fit the data to more complicated models of non-uniform resistive films.

In conclusion, the impedances of the films which we deposited are the same at the radiation frequencies of several hundred gigahertz as they are at DC, and for the purpose of making absorptive films for submillimeter bolometers, the absorption of radiation by these films is adequately described

by the standard theory, characterizing them by their impedance only. Good films can be made easily and are quite durable and stable if they are given a thin protective coating of  $\text{SiO}_2$ .

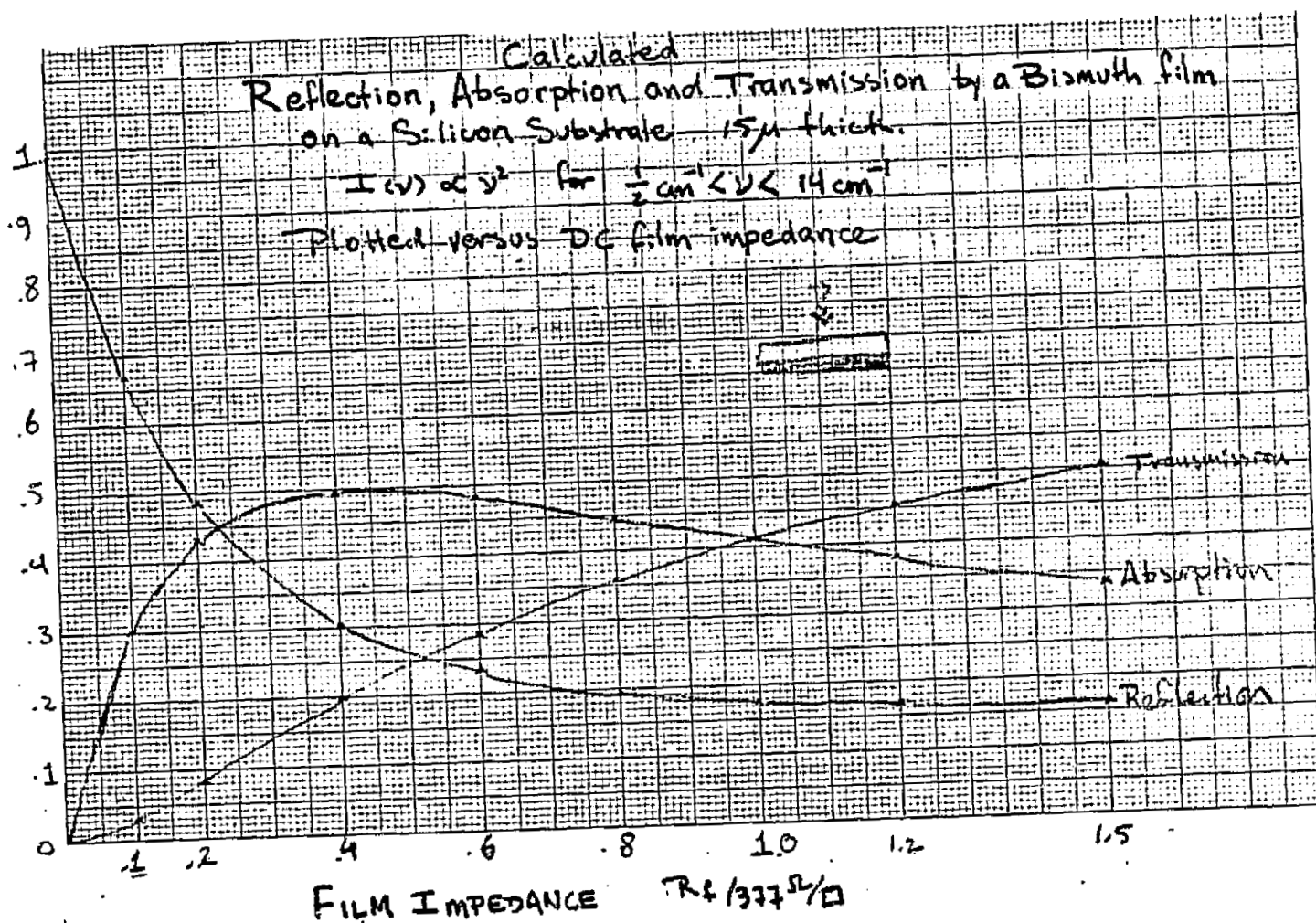


Figure 1.

ORIGINAL PAGE IS  
OF POOR QUALITY

$\eta = \mu - 1$

FIGURE 2A

# BISMUTH COATINGS ON SAPPHIRE

Residuals of Reflectivity and Transmissivity (both are fractions)

Each Point is Measurement minus Theory

Broad Band (0-35  $\text{cm}^{-1}$ )

Low Pass FILTERED (0,14  $\text{cm}^{-1}$ )

Reflectivity

Reflectivity

Transmissivity

Transmissivity

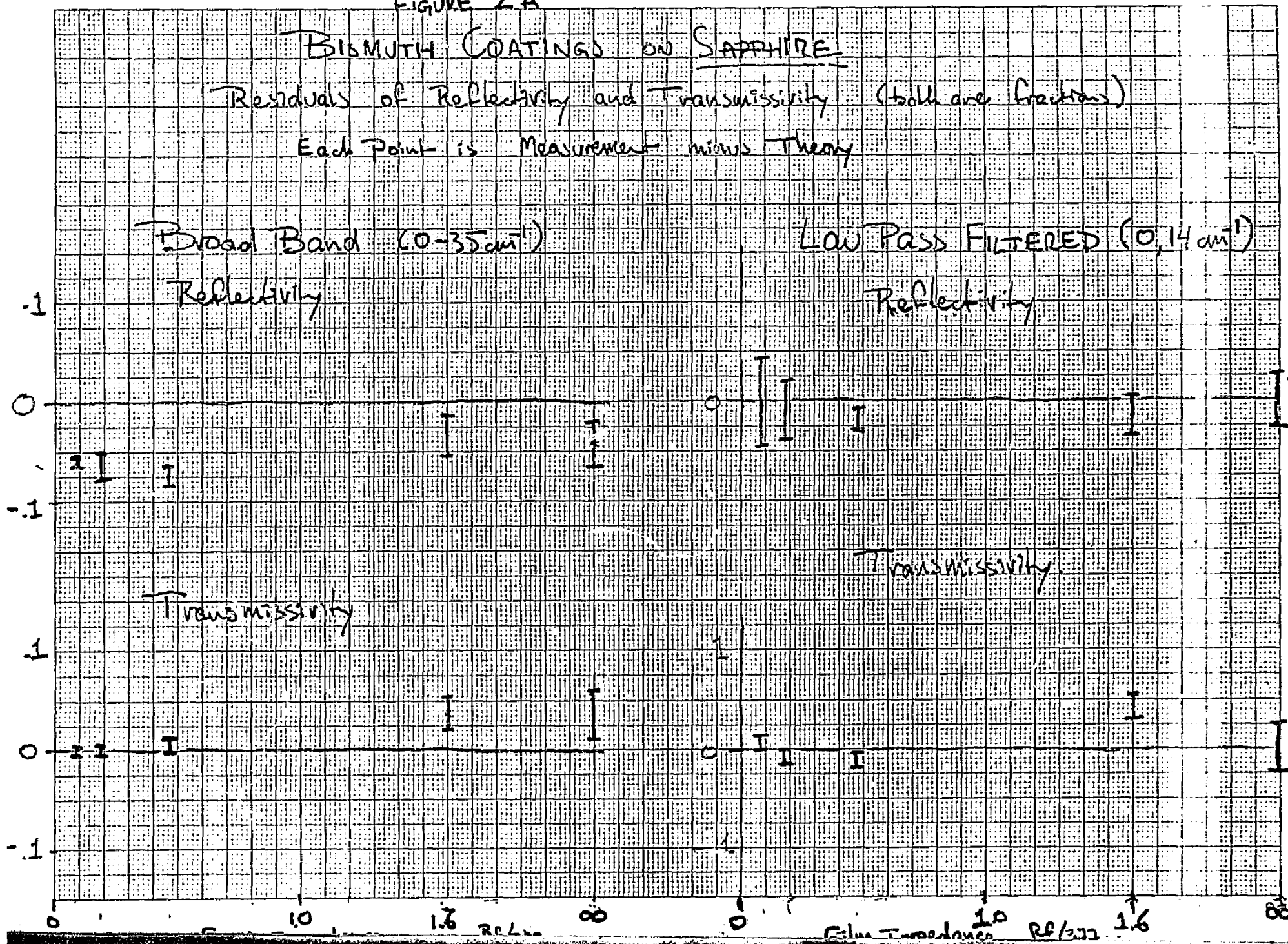
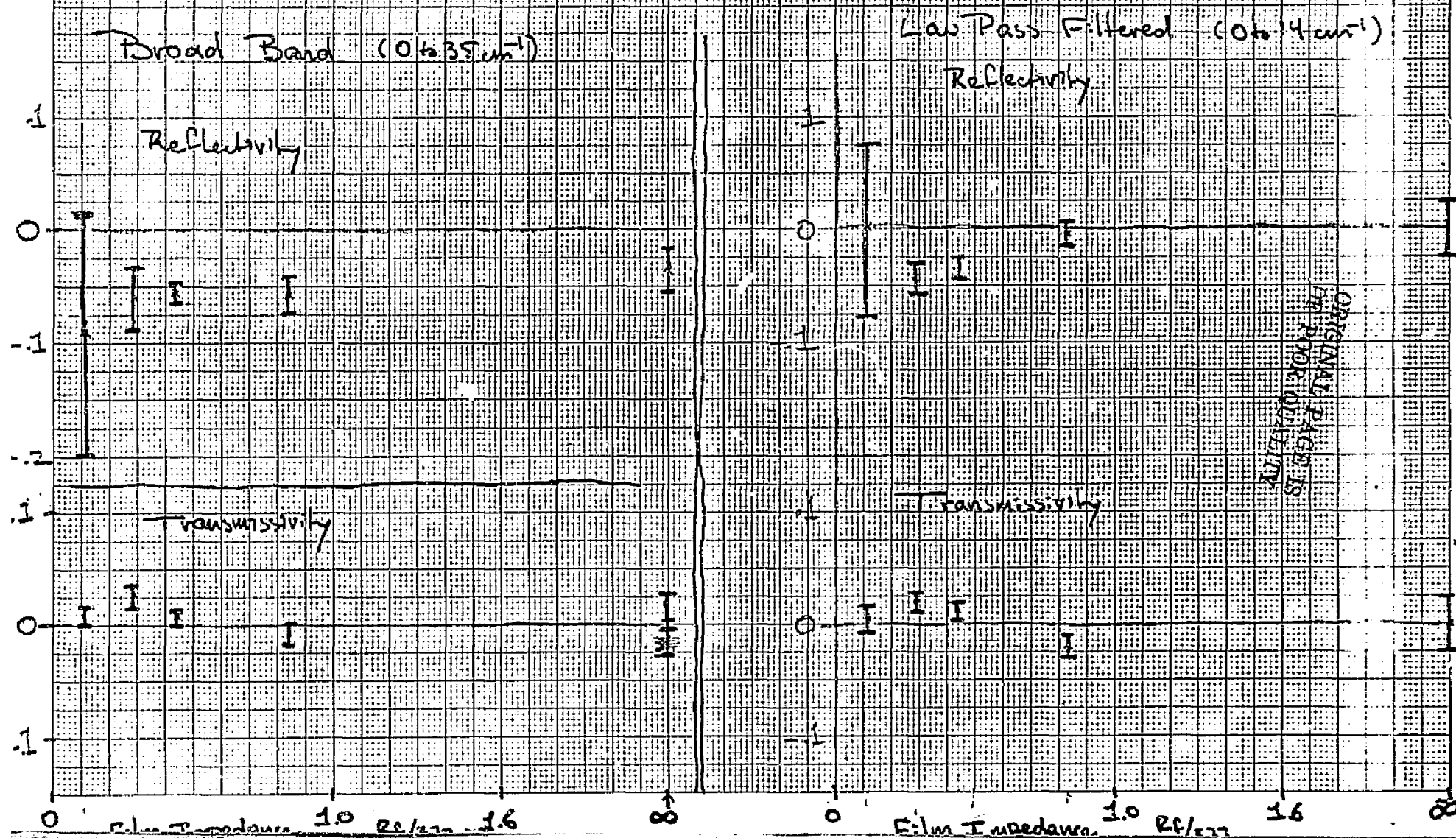


FIGURE 2B

Bismuth Coatings on Silicon

Residuals of Reflectivity and transmissivity (which are fractions)

Each Point is ~~THEORY~~ Measurement minus Theory

### Measured Reflection and Transmission by Bismuth Films on Sapphire Substrates

DC Film Impedance ( $\Omega/\square$ )	Substrate Thickness ( $\mu$ )	Input Spectrum			
		1/2 to 35 $\text{cm}^{-1}$		1/2 to 14 $\text{cm}^{-1}$	
		R	T	R	T
30	37 $\pm$ 7	.320 $\pm$ .005	.050 $\pm$ .006	.575 $\pm$ .013	.7049 $\pm$ .005
66	40 $\pm$ 4	.187 $\pm$ .005	.124 $\pm$ .006	.34 $\pm$ .01	.105 $\pm$ .005
177	33 $\pm$ 3	.215 $\pm$ .006	.230 $\pm$ .007	.26 $\pm$ .01	.223 $\pm$ .005
600	42 $\pm$ 4	.398 $\pm$ .007	.400 $\pm$ .007	.37 $\pm$ .01	.445 $\pm$ .005
$\infty$ (no Bi)	30 $\pm$ 2	.503 $\pm$ .003	.490 $\pm$ .005	.40 $\pm$ .005	.600 $\pm$ .007

### Measured Reflection and Transmission by Bismuth films on Silicon Substrates

DC Film Impedance ( $\Omega/\square$ )	Substrate Thickness ( $\mu$ )	Input Spectrum			
		1/2 to 35 $\text{cm}^{-1}$		1/2 to 14 $\text{cm}^{-1}$	
		R	T	R	T
40.3	25 $\pm$ 5	.320 $\pm$ .007	.072 $\pm$ .003	.555 $\pm$ .007	.050 $\pm$ .005
108	13 $\pm$ 3	.300 $\pm$ .005	.182 $\pm$ .003	.345 $\pm$ .005	.170 $\pm$ .007
165	14 $\pm$ 2	.245 $\pm$ .007	.235 $\pm$ .003	.255 $\pm$ .007	.237 $\pm$ .007
308	13 $\pm$ .5	.200 $\pm$ .005	.335 $\pm$ .002	.185 $\pm$ .005	.355 $\pm$ .007
$\infty$ (no Bi)	13 $\pm$ 1	.306 $\pm$ .005	.668 $\pm$ .003	.160 $\pm$ .007	.820 $\pm$ .008

Figure 3.

# EXPERIMENTAL APPARATUS

8 SAMPLES ARE ROTATED THROUGH THE  
LIGHT PIPE ONE AT A TIME.

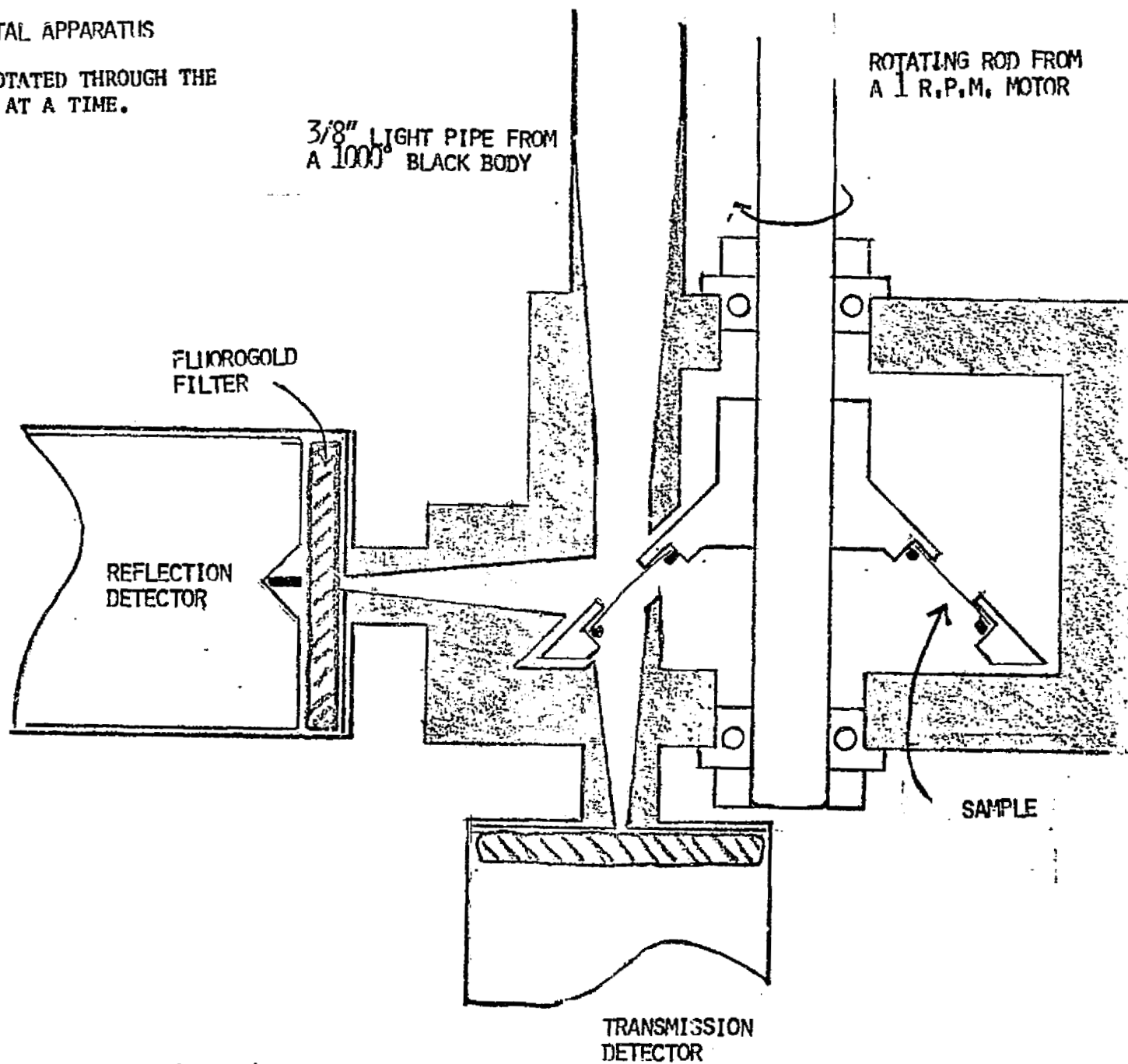


Figure 4.

ORIGINAL PAGE IS  
OF POOR QUALITY



References:

1. N. S. Nishioka, P. L. Richards, and D. P. Woody  
Applied Optics Vol. 17 No. 10 15 May 1978
2. P. M. Downey, Private Communication
3. S. Ramo and J. R. Whinnery. Fields and Waves in Modern Radio J. Wiley & Sons, New York, 1953
4. Y. S. Touloukian and E. H. Buyco, Eds. Thermophysical Properties & Matter IFI/Plenum, New York, 1970.